Journal of Atmospheric and Solar-Terrestrial Physics 71 (2009) 1093–1102

Contents lists available at ScienceDirect

Journal of Atmospheric and Solar-Terrestrial Physics

journal homepage: www.elsevier.com/locate/jastp

Ring current development during high speed streams

V.K. Jordanova [a,], H. Matsui [b], P.A. Puhl-Quinn [b], M.F. Thomsen [a], K. Mursula [c], L. Holappa [c]

[a] Los Alamos National Laboratory, Los Alamos, NM 87545, USA
[b] Space Science Center, University of New Hamsphire, Durham, NH 03824, USA
[c] Department of Physical Sciences, University of Oulu, Oulu, Finland

article info

Article history:
Accepted 29 September 2008
Available online 29 October 2008

Keywords:
Inner magnetosphere
Magnetic storms
Electric fields and ring current
Plasma motion
Plasma convection

abstract

Episodes of southward (B_z 0 0) interplanetary magnetic field (IMF) which lead to disturbed geomagnetic conditions are associated either with coronal mass ejections (CMEs) and possess long and continuous negative IMF B_z excursions, or with high speed solar wind streams (HSS) whose geoeffectiveness is due to IMF B_z profiles fluctuating about zero with various amplitudes and duration. We simulate ring current evolution during a HSS-driven storm that occurred during 24–26 October 2002 and compare its dynamics with a CME-driven storm of similar strength during 22–23 April 2001. We use our kinetic ring current–atmosphere interactions model (RAM), and investigate the mechanisms responsible for trapping particles and for causing their loss. Ring current evolution depends on the interplay of time-dependent inflow of plasma from the magnetotail, particle acceleration and loss (mainly due to charge exchange) along adiabatic drift paths, and outflow of plasma from the dayside magnetopause; all of these processes are incorporated in our model. We compare results from simulations using a newly developed, Cluster data based, University of New Hampshire inner magnetospheric electric field (UNH–IMEF) convection model with simulations using a Volland–Stern (V–S) type convection model. We find that, first, periods of increased magnetospheric convection coinciding with enhancements of plasma sheet density are needed for strong ring current buildup. Second, during the HSS-driven storm the convection potential from UNH–IMEF model is highly variable and causes sporadic shallow injections resulting in a weak ring current. The long period of enhanced convection during the CME-driven storm causes a continuous ion injection penetrating to lower L shells and stronger ring current buildup. V–S model predicts larger ring current injection during both storms. Third, the RAM driven by either convection model underestimates the total ring current energy during the recovery phase of the HSS storm, thus indicating that additional injections from substorm-induced electric fields and/or radial diffusion are needed to better reproduce its several-day long geomagnetic activity.

Published by Elsevier Ltd.

1. Introduction

Geomagnetic storms, which are some of the most important space weather phenomena, have their origin in the structure and dynamics of the solar atmosphere. The majority of large geomagnetic storms are driven by interplanetary coronal mass ejections (CMEs) associated with huge eruptions from the Sun of plasma and magnetic flux (e.g., Gosling et al., 1991; Tsurutani and Gonzalez, 1997; Richardson et al., 2001). The immediate cause of these magnetic storms at Earth is related to long periods of strong southward interplanetary magnetic field (IMF) reconnecting with the terrestrial magnetic field and allowing transfer of solar wind energy into the magnetosphere. Previous

Corresponding author. Tel.: +1 505 667 9908; fax: +1 505 665 7395.
E-mail address: vania@lanl.gov (V.K. Jordanova).

1364-6826/$ - see front matter Published by Elsevier Ltd.
doi:10.1016/j.jastp.2008.09.043

research has focused on this type of magnetic storms; they are usually larger and more frequent during solar maximum. The other type consists of magnetic storms driven by high speed streams (HSS) emanating from coronal holes (e.g., Burlaga and Lepping, 1977; Gonzalez et al., 1999); these conditions usually dominate the interplanetary (IP) medium during the declining phase of the solar cycle and solar minimum. The sporadic southward magnetic field components of HSS generate magnetic storms at Earth through magnetic reconnection as well. The magnitude of these storms is usually smaller, with average Dst 50 nT (Richardson et al., 2006), so these storms have not been considered as geoeffective and have not received much attention until recently (e.g., Tsurutani et al., 2006; Denton et al., 2006). HSS storms, however, are very effective in enhancing the electron fluxes in the outer radiation belt (e.g., Miyoshi and Kataoka, 2008). Due to the extended period of geomagnetic activity persisting for several days, Turner et al. (2006) argued that the energy input to the magnetosphere during HSS is comparable to the energy input during CMEs.

Although rarely, HSS-driven storms do reach Dst þ 100 nT. From a sample of events during 1972–1995 and 1996–2005, Richardson et al. (2006) estimated the maximum strength of this type of storms to be Dst 160 nT. The present study investigates geomagnetic activity during the 24–26 October 2002 storm (Dst 100 nT) driven by a HSS. We simulate ring current dynamics during this storm using our global ring current–atmosphere interactions model (RAM). The plasma inflow from the magnetotail is inferred from measurements from the hot plasma instruments on the Los Alamos National Laboratory (LANL) spacecraft at geosynchronous orbit. To simulate inner magnetospheric convection we use for the first time the newly developed University of New Hampshire Inner Magnetospheric Electric Field (UNH–IMEF) model from Cluster data (Matsui et al., 2004, 2008; Puhl-Quinn et al., 2008). We study inner magnetospheric dynamics obtained with this model in comparison with those obtained with the traditional Volland–Stern (V–S) model (Volland, 1973; Stern, 1975). We calculate the total energy content of the ring current and compare its temporal evolution with the Dst and the new Dxt (Karinen and Mursula, 2005) indices. Ring current energization and spatial distribution are presented through the storm, and their dependence on IP conditions is discussed. The results are compared with the simulations of the 22–23 April 2001 storm of similar strength driven by a CME.

2. Observations

The IP parameters during 23–26 October 2002 measured by the instruments on the ACE satellite are shown in Fig. 1 (left). The IP medium shows a stream–stream interaction between 30 and 36 h, where a fast stream (speed 700 km=s) overtakes a slower stream (speed 400 km=s). The HSS interface occurs at 33 h and is marked by the vertical dashed line, ahead of which the solar wind proton density and IMF are enhanced. The interplanetary electric field (IEF) shown in Fig. 1e is defined as in Hairston et al. (2003):

$$\mathrm{IEF} = V\sqrt{B_y^2 + B_z^2}\sin^2(\theta y/2), \quad (1)$$

where V is the solar wind speed, B_y and B_z are the Y and Z components of the IMF in the GSM coordinates, and y is the IMF clock angle, i.e., $y = \tan^{-1}(B_y/B_z)$. The IEF is an important driver of geomagnetic activity and is used to parameterize the UNH–IMEF model (Matsui et al., 2004, 2008). During 23–26 October it is highly fluctuating but remains enhanced above 2 mV=m in the vicinity of, and following the stream interface. Fig. 1f shows that the storm has a step-like Dst profile reaching minimum Dst = 98 nT at 45 h. This Dst index has been calculated at the World Data Center at Kyoto, Japan, using data from four observatories at low to mid-latitudes. The Dxt index shown with a dash–dotted line is an extension of the 4-station Dxt index (Karinen and Mursula, 2005) to use observations from 17 low and mid-latitude stations (nine from northern, eight from southern hemisphere). As in Dxt, the disturbances of the stations are latitudinally normalized. The difference between these two indices maximizes near the stream interface and is 15 nT. The 3 h averaged planetary Kp index (Fig. 1g) reaches maximum Kp = 6^+ at 39 h, a few hours before minimum Dst.

The high density plasma in the low velocity stream and the simultaneous IMF B_z decrease below 5 nT at 24–30 h cause the initial phase of the magnetic storm. During passage of the interaction region the driving of the magnetosphere is mainly through the large negative B_z excursions, reaching peak values of approximately 15 nT right at the leading edge of the HSS at 35 h; the maximum IEF 6 mV=m is attained at 36 h. In the high-speed flow behind the interaction region the north–south component B_z is highly fluctuating with a peak-to-peak amplitude of 5 nT causing significant Dst and Kp activity for several days.

Very different IP conditions occur during the 21–23 April 2001 CME-driven storm (Fig. 1, right). In contrast to the HSS-driven storm, an IP shock is observed at 16 h, marked by the vertical dashed line. Behind the shock the density and total field increase, and the solar wind speed reaches values of 400 km=s. At 25 h, as discussed by Jordanova et al. (2006), ACE enters a region with strong fields and a relatively smooth south-to-north IMF B_z excursion characteristic of a magnetic cloud (e.g., Burlaga et al., 1981). The B_z component decreases to about 15 nT at 34.5 h and the IEF peaks at 5 mV=m. The intense and long duration southward field of the magnetic cloud triggers a geomagnetic storm at Earth with a 15 h long main phase, gradually decreasing Dst reaching minimum Dst = 102 nT at 40 h, maximum Kp = 6^+, and a storm recovery lasting more than a day. The Dxt index is larger by 15 nT than the Dst during the recovery phase near 50 h, but otherwise the difference between these two indices is small for this CME storm.

3. Model description

We simulate the development of the ring current using our global physics-based RAM (Jordanova et al., 1997, 2001) which solves the bounce-averaged kinetic equation

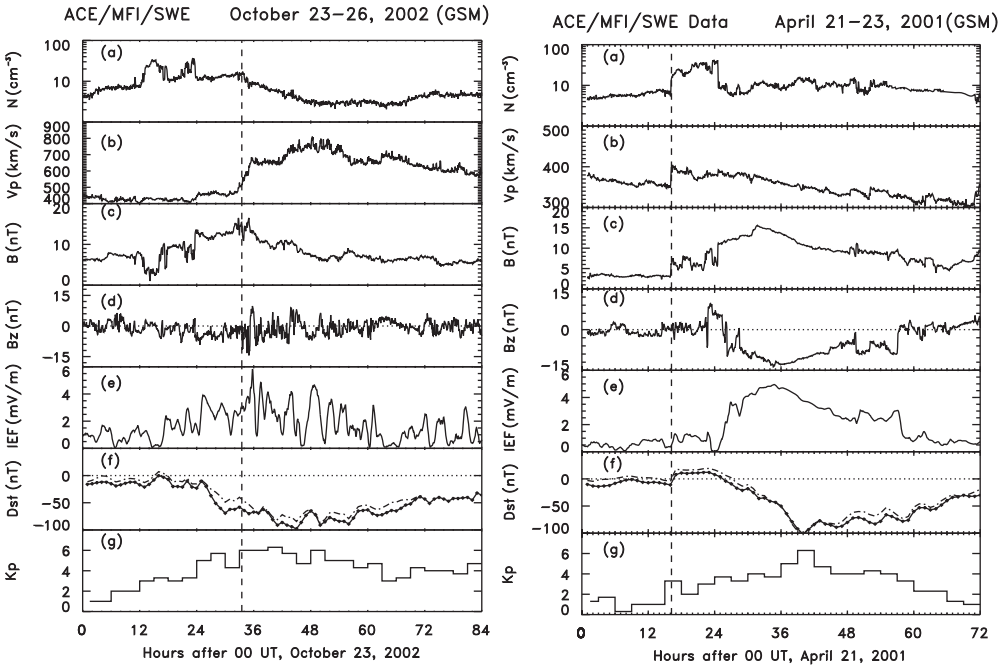

Fig. 1. (Left) Interplanetary observations from the MFI and SWEPAM instruments on ACE during 23–26 October 2002. From top to bottom the panels are: proton density, solar wind bulk speed, magnetic field strength, the B_z (GSM) component of the magnetic field, the interplanetary electric field, the Dst (diamond) and Dxt (dash–dotted) indices, and the planetary Kp index. The vertical dashed line indicates the HSS interface. (Right) Interplanetary observations during 21–23 April 2001. The vertical dashed line indicates the interplanetary shock driven by the CME.

for H^b; O^b, and He^b ions with kinetic energy from 100 eV to 400 keV and pitch angle from 01 to 901. A region in the equatorial plane spanning radial distances R_o from $2R_E$ to $6.5R_E$ and all magnetic local times (MLT) is considered. Losses from charge exchange with geocoronal hydrogen, Coulomb collisions with thermal plasma, precipitation of ring current ions at low altitude, and drift through the dayside boundary are included. The time-dependent transport along adiabatic drift paths is calculated in the present study using various convection electric field models described below and a dipole model of the Earth's magnetic field. The corotation potential is $U_{cor} = C/R_o$, where C is the corotation constant. The inflow of plasma from the magnetotail is modeled according to total ion flux measurements from the magnetospheric plasma analyzer (MPA) and the synchronous orbit particle analyzer (SOPA) on the geosynchronous LANL satellites 080, 084, 97A, 01A and 02A, using activity-dependent ion composition ratios inferred from the work of Young et al. (1982), and preserving the local time dependence of the data.

We developed our ring current model so that an arbitrary electric field could be used as a driver. In this study we compare results from (1) a Kp-dependent V–S electric potential model (Volland, 1973; Stern, 1975; Maynard and Chen, 1975) and (2) the UNH–IMEF model (Matsui et al., 2004; Puhl-Quinn et al., 2008) driven by IP conditions. We show the potential distributions obtained with these models for both the October 2002 and the April 2001 storms in Fig. 2 (left and right, respectively). The analytical V–S model depends on geomagnetic activity through the planetary Kp index (Fig. 1); we use a shielding factor g = 2 and zero MLT offset, which makes it symmetric about the dawn–dusk direction. It predicts the largest electric potential during the main phase of the storms when maximum Kp is observed, at 39–41 h during both storms. The UNH–IMEF model shown in Fig. 2 is derived from electric field data primarily from the Cluster satellites, merging complementary measurements from the electron drift instrument (EDI) and the electric fields and waves (EFW) instrument for more than 5 years of operation (2001–2006) (Puhl-Quinn et al., 2008). An inverse problem is solved to obtain the electric potential (Matsui et al., 2004, 2008). The merged data set is superior to either data set alone, improving the spatial coverage and including a wider range of geomagnetic activity levels. In addition, statistical results from ground radars and low altitude satellites are added inside the perigee of Cluster ($4R_E$). The merged electric field data are averaged to 5 min resolution, mapped to the magnetic equatorial plane using the model of Tsyganenko (2002), and sorted according to several ranges of the IEF values measured by ACE. The solar wind data are shifted in time with a proper propagation delay from ACE to Earth and averaged over 40 min intervals. The electric potential patterns derived from the average electric fields can be interpolated or extrapolated to any IEF values in principle, thus an empirical convection model as a function of IEF has been developed. As the IEF values are often measured at the L1 point, the model has a predictive capability. The UNH–IMEF model predicts increased electric potential for larger IEF values (Fig. 1), which occur during the main

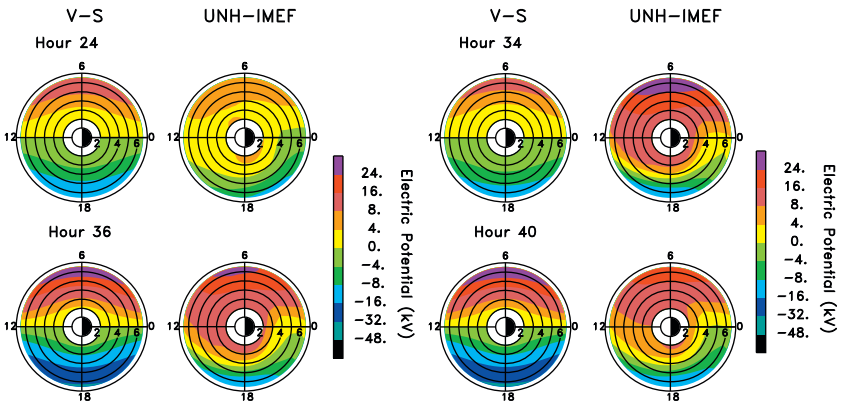

Fig. 2. Electric potentials (kV) as a function of radial distance in the equatorial plane and MLT from the Volland–Stern (V–S) and UNH–IMEF models at selected hours after 00 UT, 23 October 2002 (left) and after 00 UT, 21 April 2001 (right).

phase of the storms when IMF B_z maximizes, at 36 h during the October 2002 storm (Fig. 2, left) and 34 h during the April 2001 storm (Fig. 2, right). Realistic signatures like day–night asymmetry and skewing the potential in the postmidnight sector as in self-consistent electric field model simulations (e.g., Wolf, 1983) are seen.

4. Results and discussion

Fig. 3 (top) shows the polar cap potential drop calculated with the V–S model (dashed line) after (Stern, 1975) using 20l magnetic colatitude of the polar cap boundary, during the October 2002 and April 2001 storms (left and right, respectively). The potential drop calculated with UNH–IMEF model as the difference between the maximum and minimum potential values in a spatial domain from L ¼ 2 to 10 and all MLT is plotted with a solid line (Fig. 3, top). The UNH–IMEF model is driven by IP parameters, and during the October 2002 HSS storm predicts a highly variable potential drop, intensifying briefly to values of 60, 120, and 80 kV, at 25, 36, and 49 h, corresponding to the IEF intensifications shown in Fig. 1. During April 2001 CME storm the potential drop increases from 24 h until 34.5 h when it peaks at 90 kV; this reflects the variation of the IEF during the magnetic cloud. In contrast, the potential drop of the V–S model varies smoothly during October 2002 and reaches maximum of 105, 130, and 120 kV at 28.5, 40.5, and 49.5 h, matching the Kp intensifications (Fig. 1). During April 2001 the potential drop of the V–S model peaks at 130 kV at 40.5 h.

The plasma sheet ion density and temperature from the MPA (Fig. 3, middle) are plotted along the nightside orbit of the LANL satellites (between MLT ¼ 18 and 6) and exhibit temporal as well as spatial variations. The data indicate that: (1) the ring current source population is highly variable throughout the intervals, and (2) there is very good nightside data coverage. Enhanced density is observed during the main phase of both storms with peak values from 1 to 1:5 cm ^{3} during October 2002, and from 1.5 to 2 cm ^{3} during April 2001. During the storm recovery phase, the ion density reduces to 0:5 cm ^{3} during 25 October but remains elevated near values of 1 cm ^{3} during 23 April. The ion temperature varies between 5 and 10 keV during both storms.

We investigated ring current evolution during both storms using the convection electric field models (Fig. 2) to simulate the drift of ring current ions, and the measured ion fluxes at geosynchronous orbit for plasma boundary conditions, as described in Section 3. The total energy of H^{p} ring current ions computed as a function of time is plotted in the bottom panel of Fig. 3 using V–S (dashed) or UNH–IMEF (solid) models. To isolate the effects of magnetospheric convection, we show as well test simulations where the quiet time plasma sheet measurements at 12 h were used as constant boundary conditions (CBC) throughout the modeled period. The RAM results using V–S model with CBC (dotted) indicate that this Kp-dependent convection model causes larger ring current energization during the HSS storm (47% increase in energy) than during the CME storm (32%). In contrast, the RAM results using UNH–IMEF model with CBC (dashed–dotted) indicate that this IP-dependent convection model causes larger ring current energization during the CME storm (28% increase in energy) than during the HSS storm (23%). When the electric field decreases, the energy loss becomes predominant and the ring current decays. The proton energy remains enhanced during the recovery phase of the HSS storm with both models, while it decreases quickly during the recovery phase of the CME storm. These features are modified when time-varying plasma sheet boundary conditions are considered, the latter causing smaller-scale fluctuations and larger enhancements in ring current energy during the main phase. The density drop during the recovery phase of the October storm leads to a faster initial decay (from 50 to 56 h), while the elevated density during the recovery phase of the April storm leads to a slower ring current decay.

Additional simulation results from our RAM are shown in Fig. 4 (left) during 23–25 October 2002 and in Fig. 4

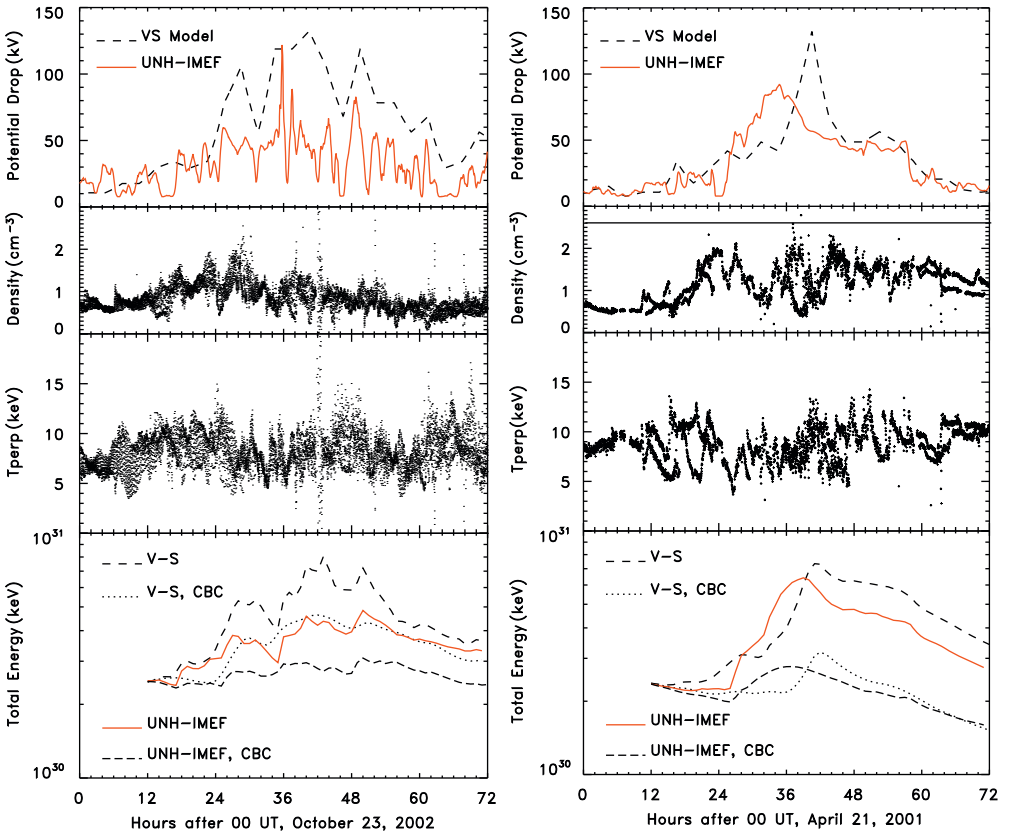

Fig. 3. (Left) Data and simulation results during 23–25 October 2002. From top to bottom the panels are: the polar cap potential drop obtained with the V–S model (dashed) and the UNH–IMEF model (solid); the nightside plasma sheet ion density, and the plasma sheet ion temperature at geosynchronous orbit; and the total H^b ring current energy using V–S (dashed) or UNH–IMEF (solid) models with time-varying boundary conditions, or V–S (dotted) or UNH–IMEF (dashed–dotted) models with constant boundary conditions (CBC). (Right) Data and simulation results during 21–23 April 2001.

(right) during 21–23 April 2001. The ring current injection rate calculated with RAM (defined as the total energy gain per hour) reflects the combined variations of the convection potential and the inflow of plasma at the nightside boundary. Several short-term intensifications occur during 24 October corresponding to the increase of the convection strength and plasma sheet density during the main phase of the HSS-driven storm (Fig. 3, left). In contrast, there is primarily one long-term enhancement on 22 April during the main phase of the CME-driven storm. This enhancement peaks at 34.5 h using UNH–IMEF model, and at 40.5 h using V–S model. The convection potential predicted with UNH–IMEF model is smaller and leads to a smaller injection rate than using V–S model (Fig. 3, right).

The energy loss rates of ring current H^b and O^b ions due to charge exchange are plotted in the middle panel of Fig. 4. Charge exchange is the major collisional loss process for ring current ions; losses due to atmospheric or Coulomb collisions are about an order of magnitude smaller (Jordanova, 2006). The loss rates reflect the time history of every storm, as the injection rates do. Their variations in time follow closely those of the total ring current energy (Fig. 3, bottom) and their magnitude is larger for H^b ions since it was the dominant ring current component during both storms. Charge exchange losses maximize during October 2002 near 31 and 44 h (Fig. 4, left), and during April 2001 near 39 h using UNH–IMEF model and near 42 h using V–S model (Fig. 4, right).

The ring current contribution to Dst index computed with RAM using the Dessler–Parker–Sckopke relation (Dessler and Parker, 1959; Sckopke, 1966) is compared with measured Dst and Dxt indices in the bottom panels of Fig. 4. Every ion injection causes an intensification of the ring current and subsequently a decrease in the calculated Dst. The ring current decays when the loss processes dominate and the injection rate becomes negative. There are thus several dips during 24 October in the simulated Dst that match very well the drops in measured Dst and Dxt. The UNH–IMEF model predicts small intermittent enhancements which are not sufficient to build a strong ring current during this HSS-driven storm. The enhancements predicted with the V–S model are larger and this model reproduces better the measured Dst index, but still overestimates its minimum by 30 nT; the agreement with the Dxt index is better.

The IP-dependent UNH–IMEF model predicts quite different temporal variation of ring current parameters during 22 April than the Kp-dependent V–S model. The UNH–IMEF model predicts a ring current injection

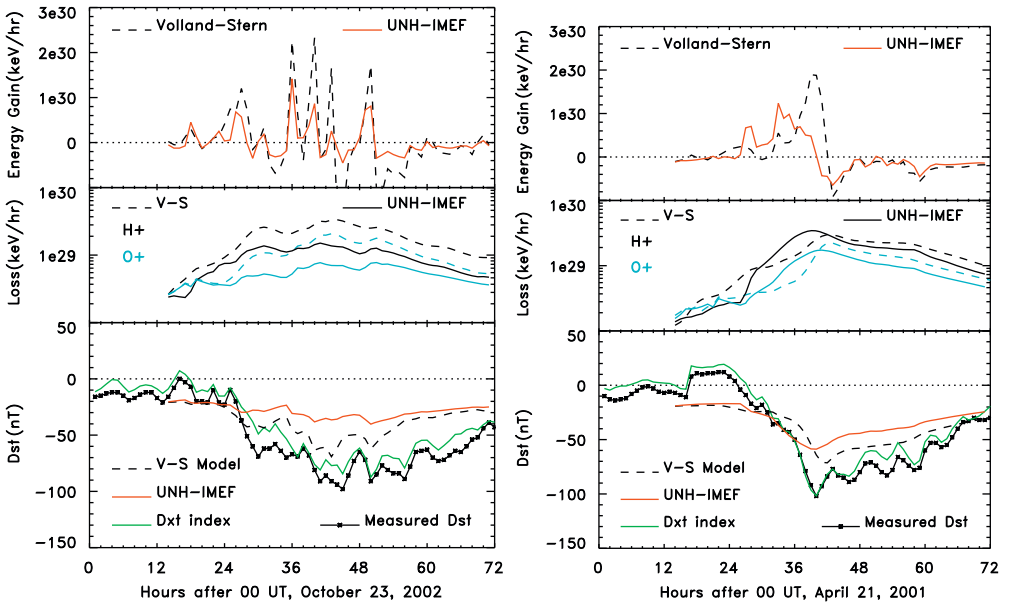

Fig. 4. (Left) Model simulations during 23–25 October 2002. From top to bottom the panels are: the calculated ring current injection rate using V–S model (dashed) and UNH–IMEF model (solid); the energy loss rate due to charge exchange for ring current H^b using V–S (dashed) or UNH–IMEF (solid) models and O^b using V–S (dashed blue) or UNH–IMEF (solid blue) models; and the computed Dst index using the two model formulations compared with measured Dst (starred line) and Dxt (dash–dot–dotted line) indices. (Right) Model simulations during 21–23 April 2001 in the same format.

maximizing near 34.5 h and reproduces very well the initial ring current buildup of this CME-driven storm; however, its convection strength drops quickly and the model underestimates ring current magnitude near minimum Dst. The enhancement of the convection potential predicted with V–S model peaks during the period of enhanced plasma sheet density and causes large ring current injection and minimum Dst 70 nT at 42 h, a few hours after measured Dst and Dxt minima. Additional injections from radial diffusion due to magnetic field fluctuations usually improve the agreement with Dst during the storm recovery phase (Jordanova et al., 2006; Jordanova, 2006). Contributions from substorm injections (Ganushkina et al., 2000), magnetotail currents (Turner et al., 2000), and ring current electrons (Jordanova and Miyoshi, 2005) could also bring better agreement with Dst and Dxt indices.

To get a further insight on ring current dynamics we traced equatorially mirroring protons in the Kp history of the October 2002 storm starting at 24 h (Fig. 5, left) and 36 h (Fig. 5, right) using a dipole magnetic field and V–S electric field. The particles are launched from a radial distance of $6.5R_E$ at various MLT and with initial energy of 7 keV, representative of the storm time plasma sheet boundary conditions. The particles are traced until they cross the dayside boundary at $10R_E$ or a maximum time of 72 h has elapsed. The corresponding energy change along each drift path is shown in the bottom panel of Fig. 5. The protons originating postmidnight spend more time in the ring current, drift inward and are more energized. Maximum energy of 45 keV is thus gained in about 6 h by a proton launched at MLT ¼ 3 (Fig. 5, left). This is consistent with the initial ring current energization and the first Dst minimum. Protons launched from the same position about 12 h later, however, do not gain much energy and quickly escape through the dayside boundary. Maximum energy of 47 keV is gained in this case by a proton launched at MLT ¼ 2 in about 4 h (Fig. 5, right).

Similar trajectory tracings of ring current protons in the Kp history of the April 2001 storm are shown in Fig. 6 (top) and the corresponding energy changes along the drift paths are plotted in Fig. 6 (bottom). In contrast to the October storm, the initial particle energization is smaller, reaching maximum of 27 keV in about 6 h for protons launched at MLT ¼ 3. This is in agreement with the slower initial ring current buildup during this storm. Particles launched in the postmidnight sector 12 h later are, however, trapped and strongly energized, reaching maximum energy of 50 keV in about 6 h, consistent with the model predicted Dst minimum at this time. As seen from the test simulations in Fig. 3 (bottom) the electric field dynamics and the subsequent acceleration and trapping of ions are only one factor needed for the storm time ring current enhancement. Another very important factor is the density of the source population, i.e., the number of particles injected at the nightside boundary. The larger plasma sheet density measured at geosynchronous (Fig. 3) during the April storm thus contributed significantly to the stronger ring current buildup compared to the October storm.

Global images of proton energy density obtained with the two electric field model formulations are shown at selected times during 24–25 October in Fig. 7 (left) and on 22 April in Fig. 7 (right). Initially ring current injections appear at high L shells on the dusk to midnight side. As the main phase of the storm proceeds, ions are

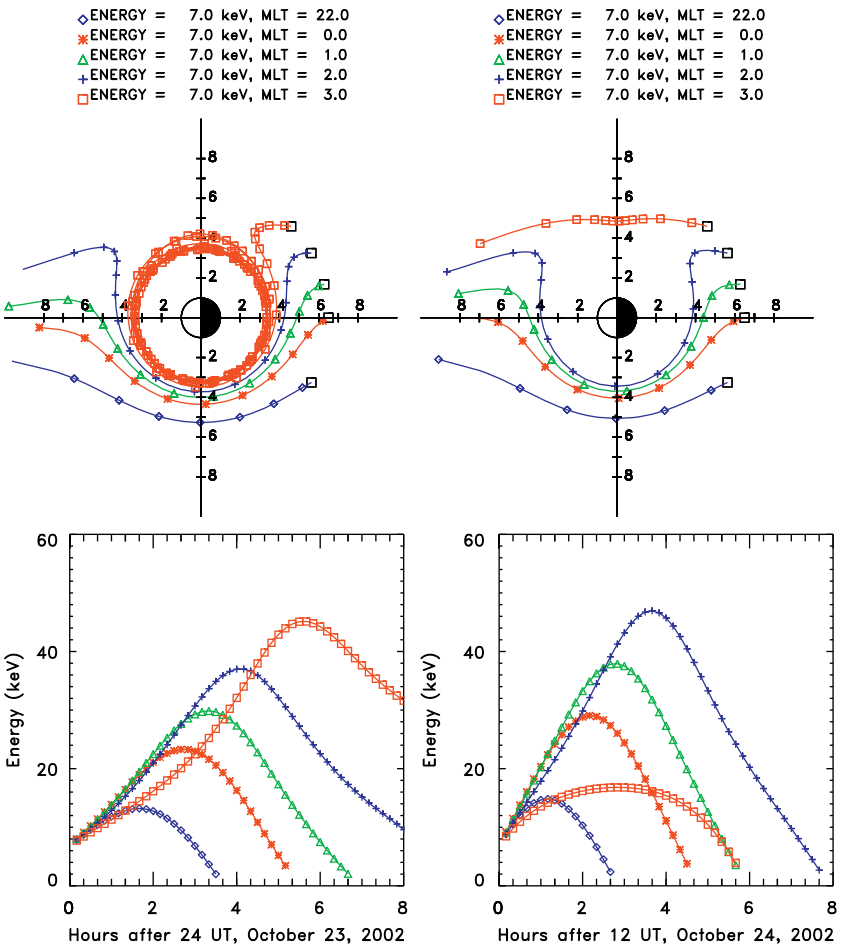

Fig. 5. (Top) Drift paths of ring current protons with 90l pitch angle in a dipole magnetic field and V–S electric field model in the Kp history of the October 2002 storm. The symbols are plotted at 30 min intervals. (Bottom) The evolution of proton energy as a function of time along each drift path with the same linestyle.

transported earthward and energized. Very asymmetric ring current energy distributions develop, the energy density being larger with the V–S model. The location of the energy density peak is predicted in the premidnight sector using V–S model. However, its location is predicted near midnight during the main phase of the April 2001 storm using UNH–IMEF model, in concurrence with previous studies using high-resolution electric potential models (e.g., Jordanova et al., 2003) or models that calculate self-consistently the electric field (e.g., Fok et al., 2003), and in better agreement with ENA observations from IMAGE satellite during this storm (e.g., Liemohn et al., 2006). An interesting feature during the HSS storm is the second peak in energy density that appears at large L due to the fresh injection of plasma sheet ions.

5. Summary and conclusions

We studied ring current dynamics during the 23–25 October 2002 storm driven by a classical stream–stream interaction region and compared them with the dynamics during the 21–23 April 2001 storm driven by a magnetic cloud. Although both storms had similar geomagnetic activity with minimum Dst 100 nT and maximum Kp ¼ 6^{þ}, they had very different IP parameters and time history. The southward B_z component of the IMF was highly fluctuating during the HSS-driven storm, leading to high temporal variations of the IEF and a step-like decreasing Dst. In contrast, the magnetic cloud exhibited a relatively smooth south-to-north B_z excursion, leading to a gradually increasing IEF and monotonically decreasing Dst.

We simulated ring current ion evolution with our RAM driven by two formulations of the electric field: (1) a Kp-dependent V–S model and (2) the IP-dependent UNH–IMEF model derived from Cluster data. A stronger potential drop was predicted by the V–S model, which caused deeper injection of ring current ions and better agreement with Dst index, but still underestimating its magnitude by 30 nT during both storms. The UNH–IMEF model had higher temporal resolution and predicted very well the initial phase of ring current buildup during the CME storm; however, its enhancement was short-lived

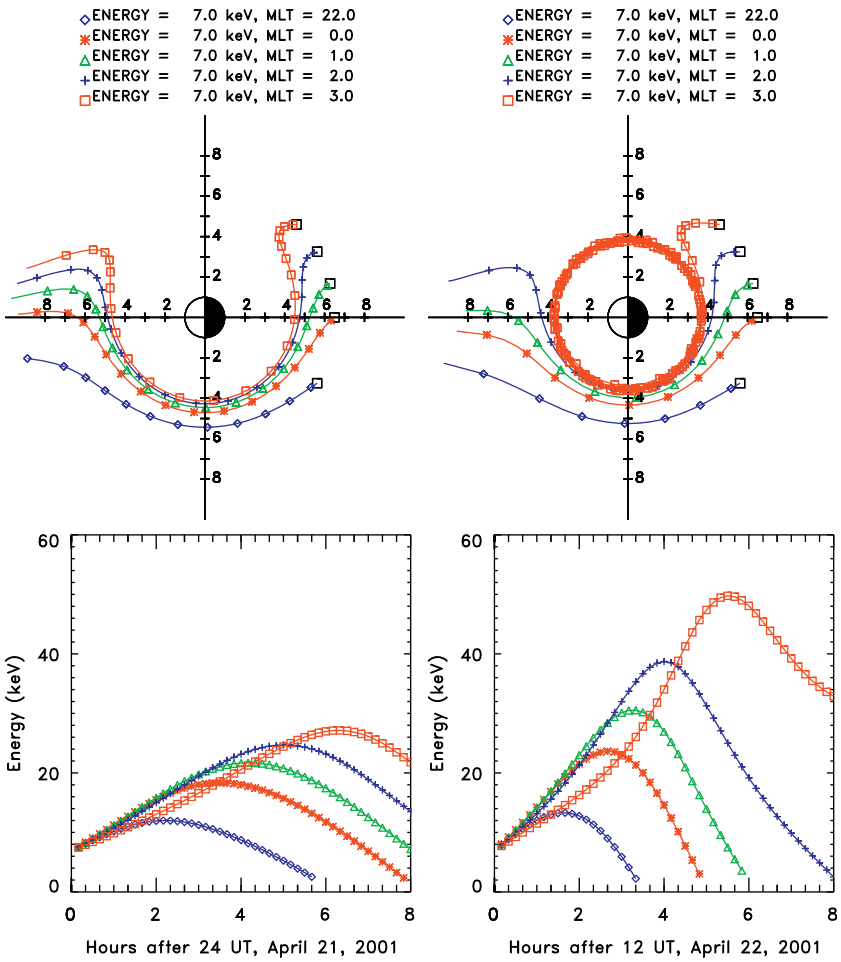

Fig. 6. (Top) Drift paths of ring current protons with 90l pitch angle in a dipole magnetic field and V–S electric field model in the Kp history of the April 2001 storm. The symbols are plotted at 30 min intervals. (Bottom) The evolution of proton energy as a function of time along each drift path with the same linestyle.

and could not produce a strong ring current. One possible reason for underestimating the Dst index by UNH–IMEF model is that the data set used to develop the model is obtained predominantly during non-storm periods; the electric fields used in the RAM are often extrapolated values. Another reason is that the inductive electric field component, which is not included in the convection models, could play a role in the energization of the ring current. These effects will be carefully considered in future studies. On the other hand, while the V–S model predicted the location of the ring current energy peak in the premidnight sector, UNH–IMEF model predicted probably a more realistic ring current asymmetry with the location of the energy density peak near midnight, in agreement with IMAGE/ENA data during the main phase of the CME storm. A second energy density peak formed at large L during the HSS storm due to fresh ion injections from the magnetotail. Such double peaks of similar strength do not appear in the RAM simulations of the CME storm.

The correlation in time between the magnitude of the convection and the plasma sheet ion density are very important for ring current evolution. The enhancement of the convection has to overlap with the enhancement of the inflow of plasma from the magnetotail for the formation of a robust ring current. Both models underpredicted the Dst minimum; they better agreed with the Dxt index, which had 15 nT smaller magnitude. The highly fluctuating IEF and plasma sheet density though reproduced well the temporal variations in Dst and Dxt during the HSS-driven storm. While the convection strength was enhanced during the recovery phase of the HSS storm, the decrease in plasma sheet density caused faster ring current decay. The elevated plasma sheet density during the recovery phase of the CME storm caused relatively slower ring current decay and better agreement with observations. Improvements of the UNH–IMEF model are currently being pursued to better capture the stronger electric fields that are not well represented when data are statistically averaged. In addition, ion composition variations at the nightside geosynchronous boundary of the RAM may not be well represented by the statistical study of Young et al. (1982)

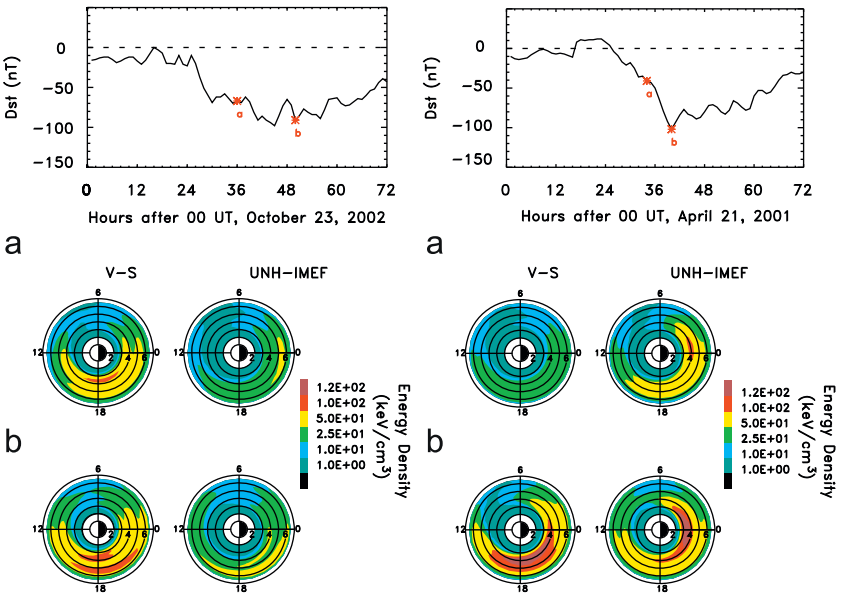

Fig. 7. Proton energy density (keV/cm^3) as a function of radial distance in the equatorial plane and MLT using V–S or UNH–IMEF models at selected hours indicated with stars on the Dst plot during 23–25 October 2002 (left) and during 21–23 April 2001 (right).

and require further investigation. In agreement with previous studies, we find that radial diffusion and substorm injections are needed in order to reproduce the long-lasting recovery phase of HSS-driven storms and these will be included in future work, as well as the electron contribution to the ring current.

Acknowledgments

Work at Los Alamos was performed under the auspices of the US Department of Energy, with partial support from the NASA LWS and GI programs, the NSF/GEM program, and from a LANL Directed Research and Development Grant. The work at UNH was supported by NASA Grant NNG05GG50G. ACE data were provided by D. McComas and N. Ness through the CDAWeb at NASA.

References

Burlaga, L.F., Lepping, R.P., 1977. The causes of recurrent geomagnetic storms. Planet Space Science 25, 1151.

Burlaga, L.F., Sittier, E., Mariani, F., Schwenn, R., 1981. Magnetic loop behind an interplanetary shock: Voyager, Helios, and IMP observations. Journal of Geophysical Research 86, 6673.

Denton, M.H., Borovsky, J.E., Skoug, R.M., Thomsen, M.F., Lavraud, B., Henderson, M.G., McPherron, R.L., Zhang, J.C., Liemohn, M.W., 2006. Geomagnetic storms driven by ICME- and CIR-dominated solar wind. Journal of Geophysical Research 111, A07S07.

Dessler, A.J., Parker, E.N., 1959. Hydromagnetic theory of geomagnetic storms. J. Geophys. Res. 64, 2239.

Fok, M.-C., et al., 2003. Global ENA image simulations. Space Science Review 109, 77.

Ganushkina, N.Yu., et al., 2000. Entry of plasma sheet particles into the inner magnetosphere as observed by Polar/CAMMICE. Journal of Geophysical Research 105, 25205.

Gonzalez, W.D., Tsurutani, B.T., Clua de Gonzalez, A.L., 1999. Interplanetary origin of geomagnetic storms. Space Science Review 88, 529.

Gosling, J.T., McComas, D.J., Phillips, J.L., Bame, S.J., 1991. Geomagnetic activity associated with Earth passage of interplanetary shock disturbances and coronal mass ejections. Journal of Geophysical Research 96, 7831.

Hairston, M.R., Hill, T.W., Heelis, R.A., 2003. Observed saturation of the ionospheric polar cap potential during the 31 March 2001 storm. Geophysical Research Letters 30, 1325.

Jordanova, V.K., 2006. Modeling the behavior of corotating interaction region driven storms in comparison with coronal mass ejection driven storms. In: Tsurutani, B.T., Gonzalez, W.D., et al. (Eds.), Recurrent Magnetic Storms: Corotating Solar Wind Streams. Geophysical Monograph Series, vol. 167. AGU, Washington DC, p. 77.

Jordanova, V.K., Miyoshi, Y., 2005. Relativistic model of ring current and radiation belt ions and electrons: initial results. Geophysical Research Letters 32, L14104.

Jordanova, V.K., Kozyra, J.U., Nagy, A.F., Khazanov, G.V., 1997. Kinetic model of the ring current–atmosphere interactions. Journal of Geophysical Research 102, 14279.

Jordanova, V.K., Kistler, L.M., Farrugia, C.J., Torbert, R.B., 2001. Effects of inner magnetospheric convection on ring current dynamics: March 10–12, 1998. Journal of Geophysical Research 106, 29705–29720.

Jordanova, V.K., Boonsiriseth, A., Thorne, R.M., Dotan, Y., 2003. Ring current asymmetry from global simulations using a high-resolution electric field model. Journal of Geophysical Research 108, 1443.

Jordanova, V.K., Miyoshi, Y.S., Zaharia, S., Thomsen, M.F., Reeves, G.D., Evans, D.S., Mouikis, C.G., Fennell, J.F., 2006. Kinetic simulations of ring current evolution during the geospace environment modeling challenge events. Journal of Geophysical Research 111, A11S10.

Karinen, A., Mursula, K., 2005. A new reconstruction of the Dst index for 1932–2002. Annales de Geophysique 23, 475.

Liemohn, M.W., Ridley, A.J., Kozyra, J.U., Gallagher, D.L., Thomsen, M.F., Henderson, M.G., Denton, M.H., Brandt, P.C., Goldstein, J., 2006. Analyzing electric field morphology through data-model comparisons of the geospace environment modeling inner magnetosphere/storm assessment challenge events. Journal of Geophysical Research 111, A11S11.

Matsui, H., Jordanova, V.K., Quinn, J.M., Torbert, R.B., Paschmann, G., 2004. Derivation of electric potential patterns in the inner magnetosphere from Cluster EDI data: initial results. Journal of Geophysical Research 109, A10202.

Matsui, H., Puhl-Quinn, P.A., Jordanova, V.K., Khotyaintsev, Y., Lindqvist, P.-A., Torbert, R.B., 2008. Derivation of inner magnetospheric electric field (UNH–IMEF) model using Cluster data set. Annales de Geophysique 26, 2887.

Maynard, N.C., Chen, A.J., 1975. Isolated cold plasma regions: observations and their relation to possible production mechanisms. Journal of Geophysical Research 80, 1009.

Miyoshi, Y., Kataoka, R., 2008. Flux enhancement of the outer radiation belt electrons after the arrival of stream interaction regions. Journal of Geophysical Research 113, A03S09.

Puhl-Quinn, P.A., Matsui, H., Jordanova, V.K., Khotyaintsev, Y., Lindqvist, P.-A., 2008. An effort to derive an empirically based, inner-magnetospheric electric field model: merging Cluster EDI and EFW data. Journal of Atmospheric and Solar-Terrestrial Physics 70, 564.

Richardson, I., Cliver, E., Cane, H., 2001. Sources of geomagnetic storms for solar minimum and maximum conditions during 1972–2000. Geophysical Research Letters 28, 2569.

Richardson, I.G., et al., 2006. Major geomagnetic storms (Dst p ?100 nT) generated by corotating interaction regions. Journal of Geophysical Research 111, A07S09.

Sckopke, N., 1966. A general relation between the energy of trapped particles and the disturbance field over the Earth. J. Geophys. Res. 71, 3125.

Stern, D.P., 1975. The motion of a proton in the equatorial magnetosphere. Journal of Geophysical Research 80, 595.

Tsurutani, B.T., Gonzalez, W.D., 1997. The interplanetary causes of magnetic storms: a review. In: Tsurutani, B.T., Gonzalez, W.D., Kamide, Y., Arballo, J.K. (Eds.), Magnetic Storms. Geophysical Monograph Series, vol. 98. AGU, Washington, DC, p. 77.

Tsurutani, B.T., McPherron, R.L., Gonzalez, W.D., Lu, G., Sobral, J.H.A., Gopalswamy, N., 2006. Recurrent Magnetic Storms: Corotating Solar Wind Streams. Geophysical Monograph Series, vol. 167. AGU, Washington, DC.

Tsyganenko, N.A., 2002. A model of the near magnetosphere with a dawn–dusk asymmetry 1. Mathematical structure. Journal of Geophysical Research 107, 1179.

Turner, N.E., Baker, D.N., Pulkkinen, T.I., McPherron, R.L., 2000. Evaluation of the tail current contribution to Dst. Journal of Geophysical Research 105, 5431.

Turner, N.E., Mitchell, E.J., Knipp, D.J., Emery, B.A., 2006. Energetics of magnetic storms driven by corotating interaction regions: a study of geoeffectiveness. In: Tsurutani, B.T., McPherron, R., Gonzalez, W., Lu, G., Sobral, J.H.A., Gopalswamy, N. (Eds.), Recurrent Magnetic Storms: Corotating Solar Wind Streams. Geophysical Monograph Series, vol. 167. AGU, Washington, DC, p. 113.

Volland, H., 1973. A semiempirical model of large-scale magnetospheric electric fields. Journal of Geophysical Research 78, 171.

Wolf, R.A., 1983. The quasi-static (slow-flow) region of the magnetosphere. In: Carovillano, R.L., Forbes, J.M (Eds.), Solar-Terrestrial Physics, D. Reidel, Norwell, MA, pp. 303–368.

Young, D.T., Balsiger, H., Geiss, J., 1982. Correlations of magnetospheric ion composition with geomagnetic and solar activity. Journal of Geophysical Research 87, 9077.